The morphology of Saturn's aurorae observed during the Cassini Grand Finale

A. Bader[1], S. W. H. Cowley[2], S. V. Badman[1], L. C. Ray[1], J. Kinrade[1], B. Palmaerts[3], W. R. Pryor[4]

[1]Department of Physics, Lancaster University, Lancaster, UK
[2]Department of Physics and Astronomy, University of Leicester, Leicester, UK
[3]Laboratoire de Physique Atmosphérique et Planétaire, Space sciences, Technologies and Astrophysics Research (STAR) Institute, Université de Liège, Liège, Belgium
[4]Science Department, Central Arizona College, Coolidge, AZ, USA

Key Points:

- We present observations of Saturn's ultraviolet aurorae in unprecedented resolution, revealing previously unseen small-scale features
- The main aurorae can be smooth or rippled, likely depending on magnetospheric conditions, and multiple parallel arcs are observed near dusk
- An outer emission is, although variable in brightness, always present and suggested to be driven by hot electrons from the ring current

Corresponding author: Alexander Bader, `a.bader@lancaster.ac.uk`

Abstract

Cassini's mission exploring the Saturn system ended with the Grand Finale, a series of orbits bringing the spacecraft closer to the planet than ever before and providing unique opportunities for observations of the ultraviolet aurorae. This study presents a selection of high-resolution imagery showing the aurorae's small-scale structure in unprecedented detail. We find the main arc to vary between a smooth and a rippled structure, likely indicating quiet and disturbed magnetospheric conditions, respectively. It is usually accompanied by a diffuse and dim outer emission on its equatorward side which appears to be driven by wave-scattering of hot electrons from the inner ring current into the loss cone. The dusk side is characterized by highly dynamic structures which may be signatures of radial plasma injections. This image set will be the only high-resolution data for the foreseeable future and hence forms an important basis for future auroral research on Saturn.

Plain Language Summary

At the end of its mission, the Cassini spacecraft performed a set of orbits bringing it closer to Saturn than ever before. By passing over the planet's polar regions at such low altitude, its ultraviolet camera could observe Saturn's aurorae in unprecedented resolution. The observations show for the first time the detailed structure of the main auroral arc which varies between a smooth and a rippled shape, likely depending on how quiet or disturbed the plasma near Saturn is. We further find a host of small arcs and blobs near dusk whose origins are not readily explained with the current understanding of how Saturn's aurorae are driven. Diffuse features surrounding the brightest auroral emissions are attributed to hot electrons from the equatorial plane which are scattered such that they can reach Saturn's atmosphere. These observations are of unique quality and invaluable for future auroral studies.

1 Introduction

Saturn's ultraviolet (UV) aurorae consist of various morphological components located around the planet's poles. Some of these are rather static and long-lived, while others are more transient, indicating explosive energy release somewhere along the associated magnetic field lines.

The overall auroral morphology is typically dominated by the so called "main auroral oval" or "main emission". Located at typically 15−20° colatitude from either pole (e.g., Carbary, 2012; Bader, Badman, Kinrade, et al., 2019), equatorward of Saturn's polar hexagon in the north (Pryor et al., 2019), the relatively circular bright band of main UV emission around the pole is colocated with the infrared main aurorae (e.g., Melin et al., 2011; Badman, Achilleos, et al., 2011; Badman, Tao, et al., 2011) and expected to map to equatorial distances beyond the middle ring current (e.g., Belenkaya et al., 2014). The exact mechanism causing the acceleration of electrons into Saturn's polar ionospheres and thus generating the aurorae is unclear, but it is presumed that azimuthal flow shears between plasma populations subcorotating at different angular velocities in the outer magnetosphere may provide the required electric fields driving the observed auroral field-aligned currents (FACs) (e.g., Cowley, Bunce, & O'Rourke, 2004; Stallard et al., 2007; Talboys et al., 2009; Hunt et al., 2014; Bradley et al., 2018).

The auroral brightness varies with local time (LT), which may partly be due to the interaction of Saturn's magnetosphere with the solar wind flow. Both a static flow shear between the solar wind and magnetospheric plasma populations (e.g., Cowley, Bunce, & Prangé, 2004) and viscous interaction through Kelvin-Helmholtz (KH) waves (e.g., Delamere & Bagenal, 2010; Delamere et al., 2013) could cause asymmetries arising between the dawn and dusk aurorae. Further dynamic asymmetries are known to be imposed by the rotating patterns of FACs imposed by the two planetary period oscillation (PPO) current systems (e.g., Hunt et al., 2014; Bader et al., 2018) and frequent auroral plasma injections due to magnetotail reconnection (e.g., Mitchell et al., 2009; Radioti et al., 2016; Bader, Badman, Cowley, et al., 2019).

The main emission usually does not assume a fully closed circular shape, but consists of multiple structures subcorotating with the planet (e.g., Grodent et al., 2005). It is not centered on Saturn's magnetic/spin pole, but slightly displaced toward the midnight-dawn direction due to the compression of the dayside magnetosphere by the solar wind and the dawn-dusk differences in auroral morphology; the location of the oval is modulated about this average position by the rotating PPO current systems (e.g., Nichols et al., 2008, 2016; Bader, Badman, Kinrade, et al., 2019). Due to the significant quadrupole moment of Saturn's internal magnetic field, effectively an offset of the internal dipole field toward the northern hemisphere, the southern oval is typically larger than the northern one (e.g., Carbary, 2012; Bader, Badman, Kinrade, et al., 2019).

The structure of the main emission is highly variable. The dawn side generally features a thin well-defined arc, while the aurorae cover a wider swath in latitude post-noon. In either of those regions the arc can include interesting substructures such as "auroral beads", which are multiple detached and consecutive auroral spots located along the main emission which may be related to shear flow-ballooning instabilities (Radioti et al., 2019). Similar small isolated features are sometimes observed in the dayside aurora; Grodent et al. (2011) termed this the "bunch of grapes" configuration and proposed FACs driven by nonuniform plasma flow in the equatorial plane and vortices triggered by magnetopause KH waves as possible drivers.

Equatorward of the main aurorae a semi-permanent band of emission can often be observed, the so called "outer emission". While first observed in Hubble Space Telescope (HST) imagery near Saturn's limb (Grodent et al., 2005, 2010), the outer emission is typically too faint to exceed the HST's detection threshold on the dayside. Nevertheless, outer emission signatures were tentatively identified in some images of the most recent HST observation campaign (Lamy et al., 2018). The Cassini UVIS detector however provided many more observations (visible in, e.g., Radioti et al., 2017), which will here be exploited to further investigate this signature. It is believed to be caused by hot electrons between 7-10 R_{S} (Schippers et al., 2008) which may reach the ionosphere through pitch angle scattering by plasma waves (Grodent et al., 2010; Grodent, 2015; Tripathi et al., 2018).

In this study a selection of auroral imagery from Cassini's Grand Finale mission is presented. The orbit geometry of the spacecraft during this mission phase allowed the UVIS instrument to obtain imagery of unprecedented resolution, revealing previously unseen details of Saturn's aurorae and the high complexity of this dynamic system. Section 2 summarizes the processing methods used to obtain clean auroral imagery from the raw observation data, while sections 3 to 4 show and discuss different aspects of the observed morphology and signatures. We conclude this study in section 5 by summarizing our findings.

2 Data and methods

The far-ultraviolet channel of Cassini's UVIS instrument performed observations at wavelengths between 110-190 nm in up to 1,024 spectral bins (Esposito et al., 2004). Its 64 spatial pixels are arranged in a single line to provide an instantaneous field of view of 64×1.5 mrad. To obtain a two-dimensional image of Saturn's auroral region, this slit was moved across the region of interest by slewing the spacecraft at a slow rate while accumulating the exposure. Depending on Cassini's distance from Saturn and the viewing geometry, repeated slews across different sections of the polar region may be necessary to construct a full auroral image. The image resulting from this process is more appropriately termed a "pseudo-image", as different pixels in the final product have been imaged at different points in time. With exposure times sometimes reaching up to more than 2 hr, this is especially important to keep in mind when the dynamics of the auroral emissions are investigated.

Each pixel is projected onto a planetocentric polar grid with resolution $0.1^\circ \times 0.05^\circ$ (lon × lat) using Cassini SPICE pointing information from the NASA Planetary Data System. The projection altitude is chosen to be 1100 km above Saturn's 1-bar pressure level (defined by $R_{\mathrm{SEQ}} = 60268$ km and $R_{\mathrm{SPO}} = 54364$ km as Saturn's equatorial and polar radii), corresponding to the approximate altitude at which Saturn's aurorae are thought to be generated (Gérard et al., 2009). Finally, we obtain the estimated total unabsorbed H_2 auroral emission intensity in the 70-170 nm spectral range from the observed intensity in the UVIS FUV range by multiplying the intensity measured in the 155- to 162-nm band by a factor 8.1, as this minimizes hydrocarbon absorption effects (Gustin et al., 2016, 2017). Some dayglow usually remains in sunlit regions, but it can be removed as described in Bader, Badman, Yao, et al. (2019) if needed. Dayglow removal was only performed for the images shown in Figure 4 below.

Most images presented in this study were obtained from radial distances between 2-5 R_S, such that one UVIS pixel at the planet measures approximately 120-300 km across. This is at least comparable to three UVIS images from 2008 where a resolution of ∼200 km/pixel could be achieved (Grodent et al., 2011) and represents about a tenfold increase in resolution compared to most other UVIS images which were obtained from distances between 20-50 R_S. The HST for comparison offers a theoretical resolution of ∼150 km/pixel, but only values of >500 km/pixel can realistically be achieved due to the presence of leaking sunlight, a relatively wide point spread function and the long exposure times required due to the high detection threshold (Grodent et al., 2011). Furthermore, the usually oblique viewing geometry from Earth orbit largely limits observations to Saturn's dayside and can lead to significant pixel stretching and limb-brightening close to the terminator region (Grodent et al., 2005).

3 Dawn-dusk asymmetries of the main aurorae

The first set of images, presented in Figure 1, shows six near-complete views of the northern and southern polar auroral regions. As has already been observed in the earliest HST campaigns imaging Saturn's aurorae before the arrival of Cassini (Gérard et al., 2004, 2005), there typically is a distinct morphological difference between the dawn and dusk emissions. The region poleward of the relatively circumpolar band of variable main emission is typically dark and featureless, unlike in infrared observations where a complete infilling of the polar cap can be observed (Stallard et al., 2008). Exceptions are small patches slightly poleward of the main oval on, e.g., 2017-080/232 (Fig. 1a/d); these may be related to similar "polar dawn spots" in Jupiter's auroral emissions which appear to be signatures of internally driven magnetotail reconnection (Radioti et al., 2008, 2010). The region equatorward of the brightest aurorae often features a typically dimmer band of diffuse emission, the outer aurorae, which will be considered in more detail in the following section.

The dawn side is usually characterized by a narrow arc which, while essentially always present, shows significant variations in latitude and intensity. The latitudinal variation is thought to be controlled by the amount of open flux contained in the polar cap, by periodic displacements due to PPO FACs and by solar activity (e.g., Badman et al., 2005, 2014; Cowley et al., 2005; Bader, Badman, Kinrade, et al., 2019); the variation in intensity is less understood but seems to be influenced by solar wind conditions and PPO current systems overlaid with different transient signatures resulting from dynamic events in the magnetosphere (e.g., Bader, Badman, Cowley, et al., 2019). This auroral arc is

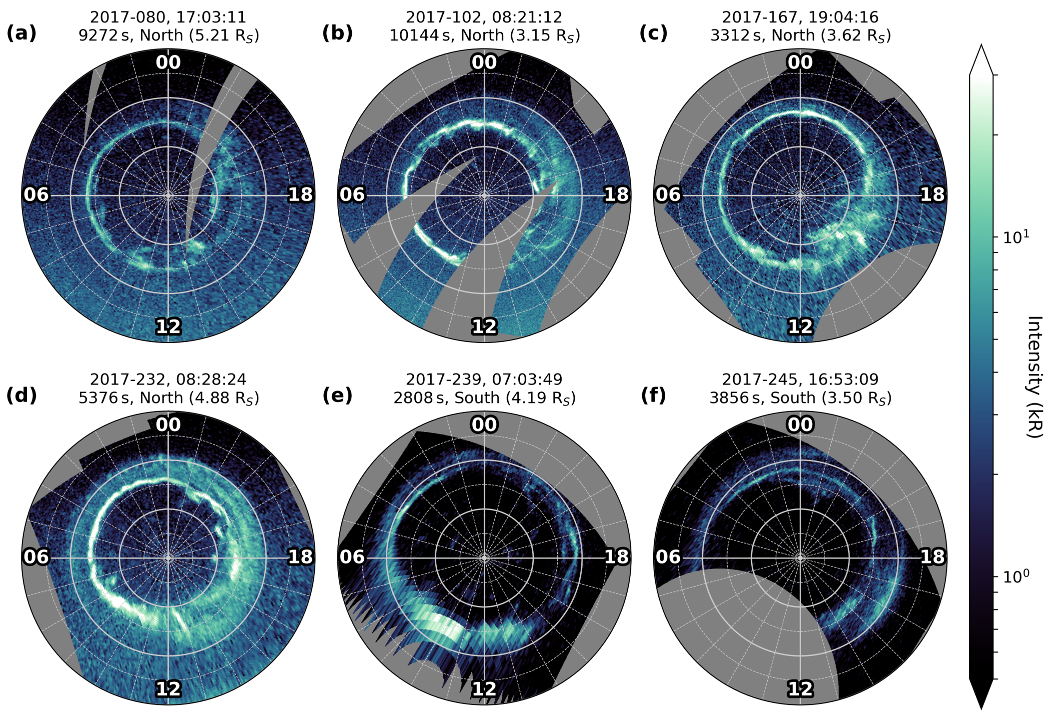

Figure 1. Selection of (nearly) full views of the (a-d) northern and (e-f) southern auroral oval obtained during Cassini's Grand Finale mission phase. The view is from above the north pole, down onto the northern or "through" the planet into the southern polar region; local noon (12 LT) is at the bottom and dawn (6 LT) at the left. Grey concentric rings mark colatitude from the pole in steps of 5°, radial lines mark local time in steps of 1 h. The images are sorted by the time of their observation; start time, exposure time, observed hemisphere and radial distance of Cassini from Saturn's surface are given at the top of each panel. The differences in background brightness (dayglow) between the northern and southern hemisphere are a seasonal effect; 2017 was a year of northern summer and southern winter.

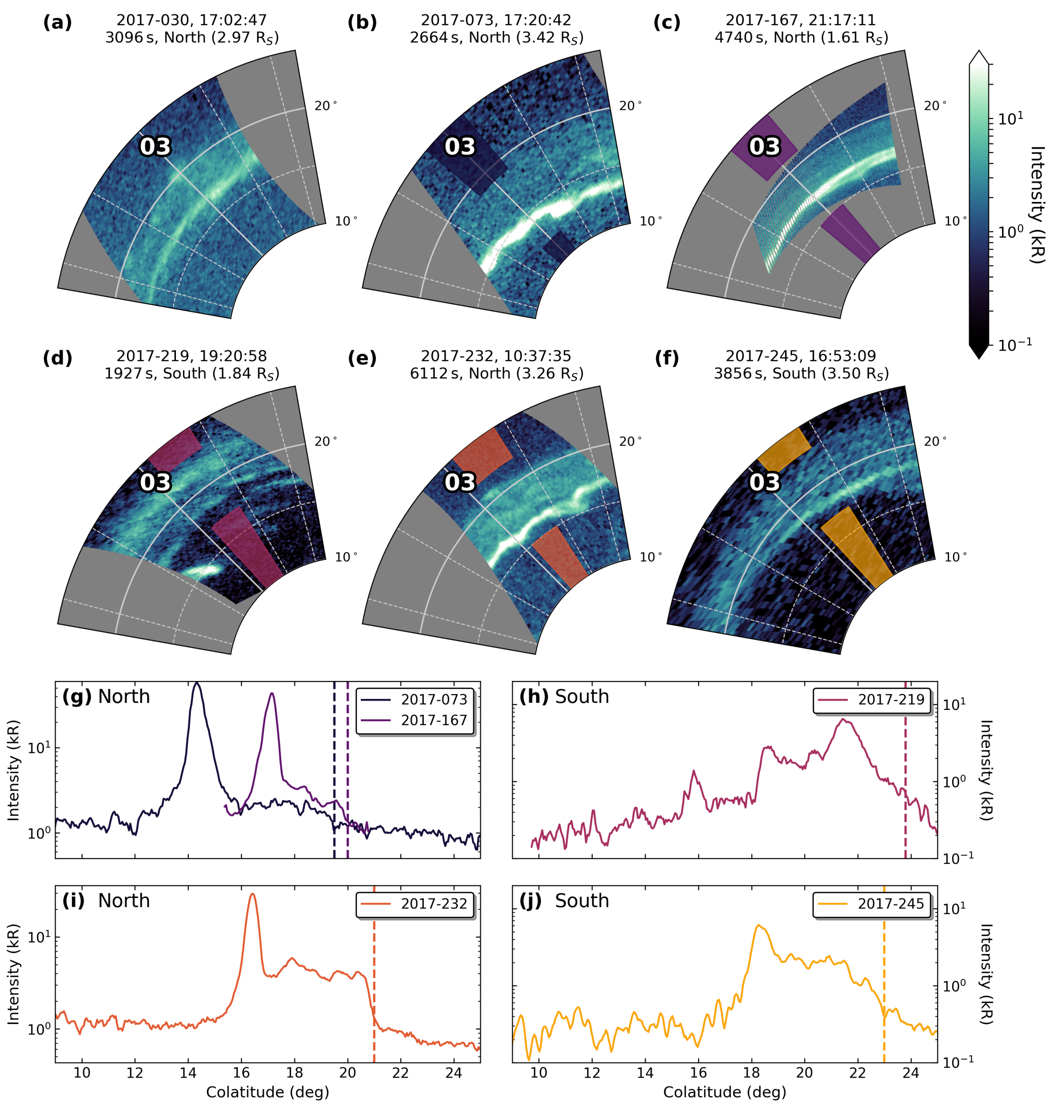

Figure 2. Selection of high-resolution imagery of Saturn's pre-dawn main auroral arc in the (a-c,e) northern and (d,f) southern hemisphere. The view is the same as in Figure 1, but now only showing part of the polar region between roughly ∼1-5 LT and 10°-25° colatitude. (g-j) Latitudinal intensity profiles of panels b-f. Shown is the intensity versus colatitude averaged within 40 min LT around the colored lines in panels (b-f). Vertical dashed lines indicate the approximate equatorward boundary of the outer emission.

thought to correspond to the layer of upward FAC seen in in situ field data in the same LT sector, which is located about 1° equatorward of the open-closed field line boundary (OCB) and may be related to a subcorotation flow shear modulated by conductivity gradients (Hunt et al., 2014; Bradley et al., 2018).

Figure 2 shows high-resolution views of the pre-dawn aurorae in both hemispheres, with panel 2c presenting the highest-resolved image of Saturn's UV aurorae obtained to date where one pixel on the planet measures ∼100 km across. Next to the main auroral arc an outer emission is discernible in all images, suggesting that it is continuously present but often too weak to be observed with HST or UVIS depending on the dayglow intensity and observation geometry. Both the main arc and the outer emission show interesting substructure, which appears to be quite variable. While, for example, panels 2a/c/f are characterized by a rather smooth and largely featureless main arc, 2b/d/e show patchy or wavy substructure which may indicate disturbed magnetospheric conditions. Even the usually rather smooth outer emission shows patchy features in 2a/e. Another interesting feature is an apparent bifurcation of the main arc in panel 2c, similar to observations of the terrestrial aurorae.

Panels 2g-j show selected latitudinal intensity profiles of these auroral images. The main auroral arc is clearly distinguishable in most cases, being brighter than surrounding emissions by about an order of magnitude in the northern hemisphere (2g/i) but only of comparable intensity in the south (2h/j). The width of the main arc (clearly discernible in the northern hemisphere, at ∼18-19° in the southern) is typically found to be just below 1° in colatitude, or ∼1000 km in the emission layer, both in the northern and southern hemisphere.

Signatures on the dusk side are of a fundamentally different nature. Instead of a defined arc, scattered patches, bifurcations and other small-scale structures indicate disturbed magnetospheric conditions thought to be controlled by the interplay between dayside reconnection activity and Vasyliūnas cycle outflow down the magnetotail. Figure 3 shows a number of high-resolution slews across the dusk aurorae (except for 3c all from the southern hemisphere) with selected colatitudinal intensity profiles shown in panels 3i-l. The emissions are structured at least down to the smallest resolvable scale of UVIS (here ∼150 km for images from the southern hemisphere); one example is a very fine arc protruding somewhat poleward in panel 3f (near ∼ 18 LT and ∼ 14° colatitude), whose full width at half maximum is ∼0.2°, or ∼200 km (see inset in 3j).

Only a few similarities can be discerned among this set of images, highlighting the great temporal variability of the system, and a clear separation of the main emission and the outer emission is not usually evident. While, for example, panels 3f-h allow the identification of a thin main arc and a dimmer, discrete outer emission on its equatorward side, emissions in the remaining images cannot easily be classified into any of the existing groups of recurrent signatures identified and investigated in previous works (e.g., Badman et al., 2015; Grodent, 2015).

Several images show single or multiple parallel arcs with various inclination across the "auroral oval". Both 2017-219 and 2017-252 exhibit four parallel arcs oriented in the near-azimuthal direction, separated by about 1-2° colatitude each (see panels 3c/i and h/l, respectively) and slightly more equatorward at their leading edge. While it is unclear whether one of the parallel arcs on 2017-219 corresponds to the main emission, the arcs' appearance equatorward of the main emission on 2017-252 and their extent reaching the equatorward edge of the diffuse emission suggests a source region in the middle magnetosphere. It is thus unlikely that they are driven by solar wind interaction at the magnetopause and related to the corresponding bifurcations observed in previous studies (e.g., Radioti et al., 2011, 2013; Badman et al., 2013).

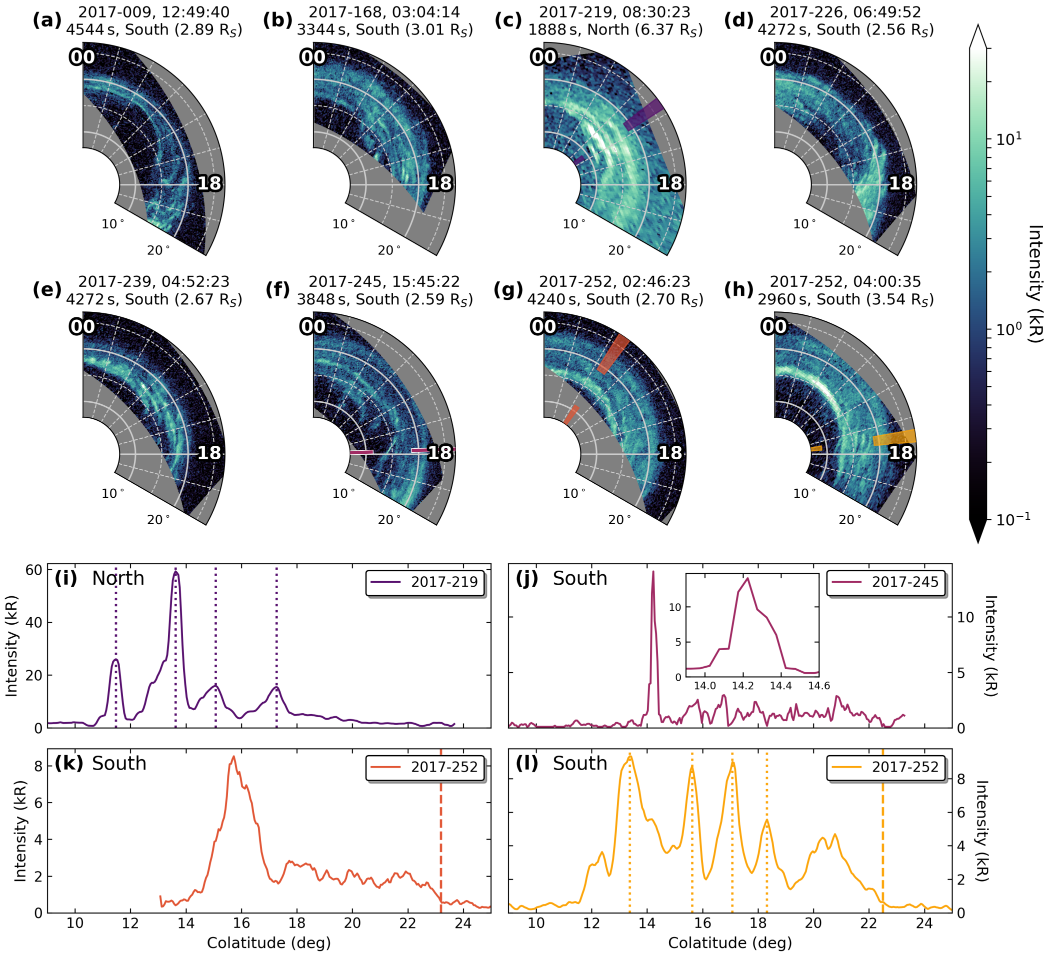

Figure 3. Selection of high-resolution imagery of Saturn's dusk auroral region in the (c) northern and (a-b,d-h) southern hemisphere. The view is the same as in Figure 1, but now only showing part of the polar region between 16-24 local time and 7-27° colatitude. (i-l) Intensity versus colatitude averaged within (i, k-l) 40 min LT (10° longitude) or (j) 1 min LT (0.25° longitude) around the colored lines in panels (c,f-h). (i,l) Parallel arcs are highlighted with dotted vertical lines. (j) An inset shows the thin intensity peak in more detail.

In panels 3a-b/d-f, sheared arcs of comparable size are visible, extending to later LTs with increasing colatitude. Auroral emissions are expected to rotate faster at larger colatitudes, as they are located on magnetic field lines which map into the magnetodisc closer to the planet where plasma rotates with a larger angular velocity (e.g., McAndrews et al., 2009; Thomsen et al., 2010; Wilson et al., 2017). An example of this differential rotation is visible when considering the fine arc in panel 3f (near $\sim$ 18 LT and $\sim$ 14° colatitude). While the arc is still rather diagonal in this image, the exposure taken directly after this image (shown in Fig. 1f) shows it to be oriented in the near-azimuthal direction. Extending this evolution backwards, it seems quite possible that this arc may have had a radial orientation initially and undergone some shearing before the first of the two images was obtained.

We propose that these sheared and azimuthal arcs, sometimes parallel to one another, may be auroral signatures of radial interchange injections. These would, similar to large-scale plasma injections triggered by magnetotail reconnection (e.g., Mitchell et al., 2009; Bader, Badman, Cowley, et al., 2019), set up localized field-aligned current systems linking to the ionosphere and cause enhanced particle precipitation, although on a much smaller scale. Additionally to their orientation and evolution, the small width of the sheared arcs appears to be comparable to the azimuthal width of injections in the equatorial plane of roughly 2°-4° longitude (e.g., Chen & Hill, 2008; Thomsen et al., 2015; Paranicas et al., 2016). However, the available auroral imagery seems to indicate a preference for these auroral features to appear near dusk while in situ observations of fresh interchange injections were shown to slightly favor the nightside (e.g., Chen & Hill, 2008; Azari et al., 2019). This is somewhat surprising as the LT preference of interchange injections and their auroral signature should be the same, but may well be an result of bias in Cassini's auroral and in situ data relating to, e.g., season or solar wind activity or the overall sparsity of observations.

4 The outer emission

Nearly all images presented up to this point have in common the presence of an outer emission. It usually seems to be more prominent on the nightside, although this may be due to its low brightness which is comparable to the intensity of dayglow on the Sun-facing side of the planet. The outer emission is typically more pronounced and spatially separated from the main emission in the southern hemisphere, whereas it forms no more than a dim, diffuse band just equatorward of the main emission in the northern hemisphere.

In general, the outer emission appears circular and centered on the spin pole in both hemispheres as visible in Figures 1 and 3. Considering the latitudinal intensity profiles shown in Figures 2g-j and 3k-l it usually has a clearly defined outer edge at $\sim$19-21° in the northern and $\sim$22-24° in the southern hemisphere (indicated with dashed vertical lines), the clear difference in northern and southern colatitudes being due to the quadrupole asymmetry. These outer boundaries map to a radial distance of $\sim$6-7 R_S in the magnetic equator plane, corresponding to the inner edge of the region of hot ion/electron plasma as determined in equatorial data (Schippers et al., 2008; Kellett et al., 2010, 2011; Carbary et al., 2018; Carbary, 2019). The "diffuse" emission observed here and in previous studies is consistent with wave-driven precipitation from this hot plasma population (Grodent et al., 2010; Tripathi et al., 2018), similar to the diffuse outer emission in Jupiter's aurorae (Radioti et al., 2009).

The poleward boundary of the outer emission typically appears to be colocated with the main aurorae. To verify whether this is true, we consider Figure 4; a quite extreme example of poleward contracted main aurorae in the northern hemisphere. The mean brightness per colatitude (all images combined to reduce noise) is shown in panel 4d. The outer emission, albeit very dim, seems to still occupy all latitudes between the main emis-

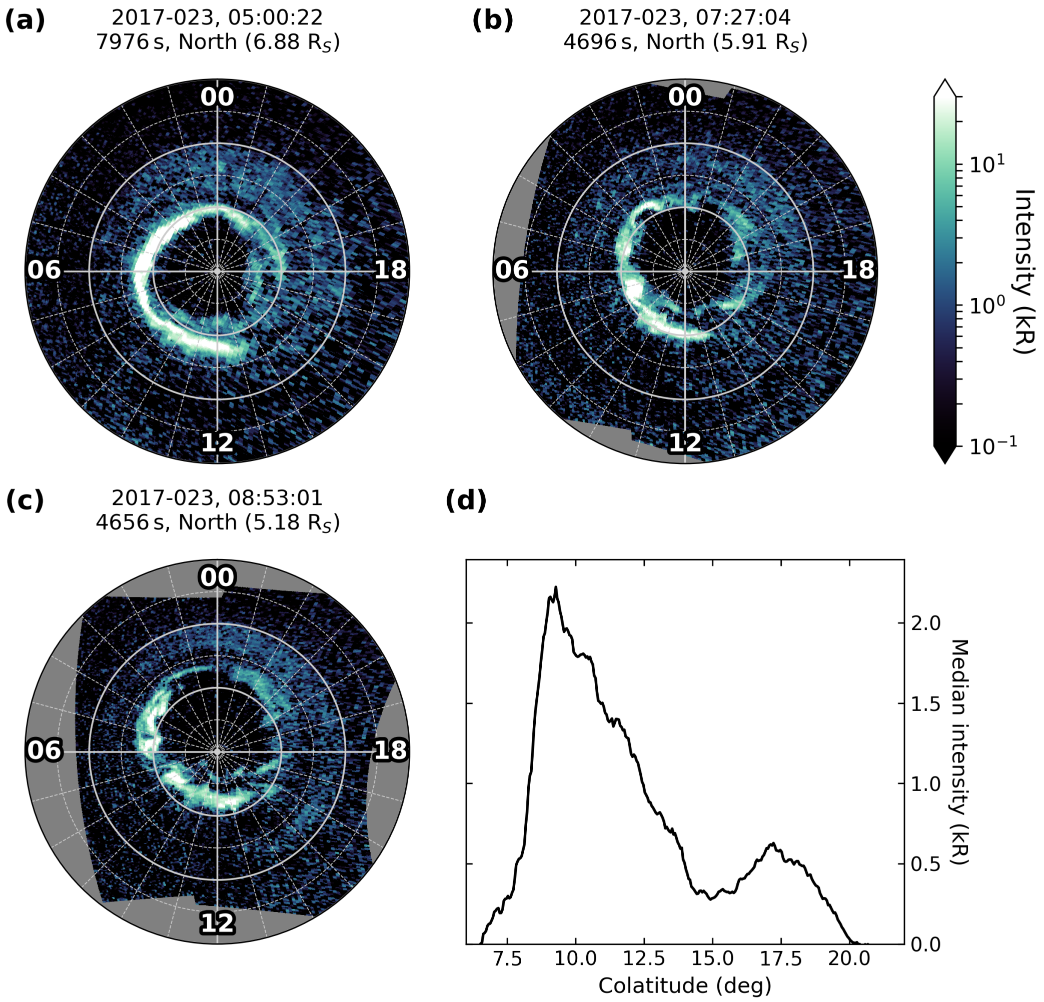

Figure 4. Observations of Saturn's outer auroral emission with the main aurorae contracted far poleward. (a-c) Images from 2017-023 with the dayglow subtracted, showing a dim and wide incomplete ring of outer emission. View is again the same as in Figure 1. (d) Average brightness per colatitude of images in panels a-c combined for all LTs. A secondary peak between 15-20° marks the outer emission, near fully detached from the main emission.

sion and its typical equatorward boundary at $\sim 20^\circ$ colatitude. There is however a dip in intensity between the main and the outer emission, similar to some observations in the southern hemisphere where the outer emission is most intense near its equatorward edge and becomes dimmer closer to the main emission (see, e.g., Figures 1f and 2d/h). This suggests that the driving mechanism of the outer emission operates throughout the ring current, but is most efficient near its planetward boundary.

It seems that the outer emission is typically weaker in the northern than in the southern hemisphere; considering the intensity profiles shown in Figures 2g-j and 3i-l, the northern outer emission reaches up to 4 kR only in exceptional cases (Fig. 2i) whereas larger intensities are observed frequently in the south (Fig. 1f, 2d/h and 3h/l). This implies that the wave diffusion responsible is "weak", i.e. the loss cone is not filled. Weak diffusion corresponds to pitch angle scattering per bounce which is less than the angular width of the loss cone, so that only the outer part of the loss cone gets filled. With the loss cone being smaller in the north than in the south as a result of the higher magnetic field strength in the north, arising from the significant quadrupole asymmetry, more particles precipitate in the south. An equivalent effect is found in the South Atlantic Anomaly at Earth (e.g., Vampola & Gorney, 1983). If the pitch angle scattering becomes "strong", meaning scattering by at least the loss cone angle in each bounce, then the loss cone will be "full" in both hemispheres, resulting in an isotropized distribution with identical precipitating flux in both hemispheres.

5 Conclusions

In this study we presented a selection of auroral images from Cassini's Grand Finale orbits, providing auroral observations of unprecedented spatial resolution in both hemispheres, and put them into context with previous results obtained in auroral studies. The data presented here reveal the amazing small-scale structure and dynamics of Saturn's UV aurorae which were usually not resolvable during earlier mission phases, and remains hidden with the limited capabilities of the HST.

Close views of the main auroral oval at pre-dawn LTs reveal that the main arc's structure is highly variable; it can be smooth or rippled and at times bifurcated. It is yet to be investigated in detail what controls this changeable behavior, but it seems reasonable to suggest that disturbed magnetospheric conditions are associated with more rippled configurations as an effect of disturbed plasma flows and density gradients in the equatorial magnetodisc.

The dusk emission was shown to be highly complex, every image exhibiting very different signatures. Recurring behavior could not readily be observed for the most part, although several observations of multiple parallel arcs with different inclination across the auroral oval were found. Their orientation and size seem to indicate they are signatures of radial interchange injections, evolving into a sheared and eventually azimuthal configuration due to the differential rotation of the magnetosphere.

Virtually all imagery obtained during the Grand Finale shows an outer emission to be present, a diffuse ring of dim aurorae just equatorward of the main emission. Based on its location and circular shape we presume that it is driven by hot electrons from the inner ring current which are scattered into the loss cone by wave activity. The interhemispheric difference in intensity and latitudinal position, owing to the significant quadrupole moment of Saturn's internal magnetic field, indicates the wave diffusion to be weak such that only a part of the loss cone is filled.

After being in orbit around Saturn for more than 13 years, these are the last auroral images from the Cassini spacecraft. They reveal previously unseen detail of Saturn's UV aurorae and perhaps prompt more questions about their origins than they can help answer - highlighting ever more the need for capable missions to planets in the outer solar system and, especially in absence of such missions to the Saturn system anytime soon, the need for comparative planetology.

Acknowledgments

All Cassini data are publicly available from the NASA Planetary Data System (`https://pds.jpl.nasa.gov`). Cassini operations are supported by NASA (managed by the Jet Propulsion Laboratory) and European Space Agency (ESA). AB was funded by a Lancaster University FST studentship. SWHC was supported by STFC grant ST/N000749/1. SVB, LCR and JK were supported by STFC grant ST/R000816/1. SVB was also supported by an STFC Ernest Rutherford Fellowship ST/M005534/1. BP acknowledges financial support from the Belgian Federal Science Policy Office (BELSPO) via the PRODEX Programme of ESA.

References

Azari, A. R., Jia, X., Liemohn, M. W., Hospodarsky, G. B., Provan, G., Ye, S., ... Mitchell, D. G. (2019, March). Are Saturn's Interchange Injections Organized by Rotational Longitude? *Journal of Geophysical Research: Space Physics*, *124*(3), 1806–1822. Retrieved 2019-08-05, from `https://onlinelibrary.wiley.com/doi/abs/10.1029/2018JA026196` doi: 10.1029/2018JA026196

Bader, A., Badman, S. V., Cowley, S. W. H., Yao, Z. H., Ray, L. C., Kinrade, J., ... Pryor, W. R. (2019, September). The Dynamics of Saturn's Main Aurorae. *Geophysical Research Letters*, *46*(17-18), 10283–10294. Retrieved 2019-10-24, from `https://onlinelibrary.wiley.com/doi/abs/10.1029/2019GL084620` doi: 10.1029/2019GL084620

Bader, A., Badman, S. V., Kinrade, J., Cowley, S. W. H., Provan, G., & Pryor, W. (2019, February). Modulations of Saturn's UV auroral oval location by planetary period oscillations. *Journal of Geophysical Research: Space Physics*, *124*(2), 952–970. Retrieved 2019-03-23, from `https://onlinelibrary.wiley.com/doi/abs/10.1029/2018JA026117` doi: 10.1029/2018JA026117

Bader, A., Badman, S. V., Kinrade, J., Cowley, S. W. H., Provan, G., & Pryor, W. R. (2018, October). Statistical planetary period oscillation signatures in Saturn's UV auroral intensity. *Journal of Geophysical Research: Space Physics*, *123*, 8459–8472. Retrieved 2018-10-30, from `http://doi.wiley.com/10.1029/2018JA025855` doi: 10.1029/2018JA025855

Bader, A., Badman, S. V., Yao, Z. H., Kinrade, J., & Pryor, W. R. (2019, April). Observations of Continuous Quasiperiodic Auroral Pulsations on Saturn in High Time-Resolution UV Auroral Imagery. *Journal of Geophysical Research: Space Physics*, *124*, 2451–2465. Retrieved 2019-05-19, from `https://onlinelibrary.wiley.com/doi/abs/10.1029/2018JA026320` doi: 10.1029/2018JA026320

Badman, S. V., Achilleos, N., Baines, K. H., Brown, R. H., Bunce, E. J., Dougherty, M. K., ... Stallard, T. (2011, February). Location of Saturn's northern infrared aurora determined from Cassini VIMS images. *Geophysical Research Letters*, *38*(L03102). Retrieved 2018-12-10, from `http://doi.wiley.com/10.1029/2010GL046193` doi: 10.1029/2010GL046193

Badman, S. V., Branduardi-Raymont, G., Galand, M., Hess, S. L. G., Krupp, N., Lamy, L., ... Tao, C. (2015, April). Auroral Processes at the Giant Planets: Energy Deposition, Emission Mechanisms, Morphology and Spectra. *Space Science Reviews*, *187*(1-4), 99–179. Retrieved 2018-05-11, from `http://link.springer.com/10.1007/s11214-014-0042-x` doi: 10.1007/s11214-014-0042-x

Badman, S. V., Bunce, E. J., Clarke, J. T., Cowley, S. W. H., Gérard, J.-C., Grodent, D., & Milan, S. E. (2005). Open flux estimates in Saturn's magnetosphere during the January 2004 Cassini-HST campaign, and implications for reconnection rates. *Journal of Geophysical Research*, *110*(A11216). Retrieved 2018-04-20, from http://doi.wiley.com/10.1029/2005JA011240 doi: 10.1029/2005JA011240

Badman, S. V., Jackman, C. M., Nichols, J. D., Clarke, J. T., & Gérard, J.-C. (2014, March). Open flux in Saturn's magnetosphere. *Icarus*, *231*, 137–145. Retrieved 2018-04-20, from http://linkinghub.elsevier.com/retrieve/pii/S0019103513005137 doi: 10.1016/j.icarus.2013.12.004

Badman, S. V., Masters, A., Hasegawa, H., Fujimoto, M., Radioti, A., Grodent, D., … Coates, A. (2013, March). Bursty magnetic reconnection at Saturn's magnetopause. *Geophysical Research Letters*, *40*(6), 1027–1031. Retrieved 2018-04-20, from http://doi.wiley.com/10.1002/grl.50199 doi: 10.1002/grl.50199

Badman, S. V., Tao, C., Grocott, A., Kasahara, S., Melin, H., Brown, R. H., … Stallard, T. (2011, December). Cassini VIMS observations of latitudinal and hemispheric variations in Saturn's infrared auroral intensity. *Icarus*, *216*(2), 367–375. Retrieved 2019-01-18, from https://linkinghub.elsevier.com/retrieve/pii/S0019103511003836 doi: 10.1016/j.icarus.2011.09.031

Belenkaya, E. S., Cowley, S. W. H., Meredith, C. J., Nichols, J. D., Kalegaev, V. V., Alexeev, I. I., … Blokhina, M. S. (2014, June). Magnetospheric magnetic field modelling for the 2011 and 2012 HST Saturn aurora campaigns - implications for auroral source regions. *Annales Geophysicae*, *32*(6), 689–704. Retrieved 2018-04-23, from http://www.ann-geophys.net/32/689/2014/ doi: 10.5194/angeo-32-689-2014

Bradley, T. J., Cowley, S. W. H., Provan, G., Hunt, G. J., Bunce, E. J., Wharton, S. J., … Dougherty, M. K. (2018, May). Field-aligned currents in Saturn's nightside magnetosphere: Subcorotation and planetary period oscillation components during northern spring. *Journal of Geophysical Research: Space Physics*, *123*, 3602–3636. Retrieved 2018-05-23, from http://doi.wiley.com/10.1029/2017JA024885 doi: 10.1029/2017JA024885

Carbary, J. F. (2012, June). The morphology of Saturn's ultraviolet aurora. *Journal of Geophysical Research: Space Physics*, *117*(A06210). Retrieved 2018-04-20, from http://doi.wiley.com/10.1029/2012JA017670 doi: 10.1029/2012JA017670

Carbary, J. F. (2019, May). A New Ring Current Model for Saturn. *Journal of Geophysical Research: Space Physics*, *124*(5), 3378–3389. Retrieved 2019-09-06, from https://onlinelibrary.wiley.com/doi/abs/10.1029/2019JA026560 doi: 10.1029/2019JA026560

Carbary, J. F., Hamilton, D. C., & Mitchell, D. G. (2018, October). Global Maps of Energetic Ions in Saturn's Magnetosphere. *Journal of Geophysical Research: Space Physics*, *123*(10), 8557–8571. Retrieved 2019-12-04, from http://doi.wiley.com/10.1029/2018JA025814 doi: 10.1029/2018JA025814

Chen, Y., & Hill, T. W. (2008, July). Statistical analysis of injection/dispersion events in Saturn's inner magnetosphere. *Journal of Geophysical Research: Space Physics*, *113*(A07215). Retrieved 2018-10-10, from http://doi.wiley.com/10.1029/2008JA013166 doi: 10.1029/2008JA013166

Cowley, S. W. H., Badman, S. V., Bunce, E. J., Clarke, J. T., Gérard, J.-C., Grodent, D. C., … Yeoman, T. K. (2005). Reconnection in a rotation-dominated magnetosphere and its relation to Saturn's auroral dynamics. *Journal of Geophysical Research*, *110*(A02201). Retrieved 2018-04-20, from http://doi.wiley.com/10.1029/2004JA010796 doi: 10.1029/2004JA010796

Cowley, S. W. H., Bunce, E. J., & O'Rourke, J. M. (2004, May). A simple quantitative model of plasma flows and currents in Saturn's polar ionosphere. *Journal of Geophysical Research*, *109*(A05212). Retrieved 2018-04-20, from http://

doi.wiley.com/10.1029/2003JA010375 doi: 10.1029/2003JA010375
Cowley, S. W. H., Bunce, E. J., & Prangé, R. (2004, April). Saturn's polar ionospheric flows and their relation to the main auroral oval. *Annales Geophysicae*, *22*(4), 1379–1394. Retrieved 2018-04-23, from http://www.ann-geophys.net/22/1379/2004/ doi: 10.5194/angeo-22-1379-2004
Delamere, P. A., & Bagenal, F. (2010, October). Solar wind interaction with Jupiter's magnetosphere. *Journal of Geophysical Research: Space Physics*, *115*(A10201). Retrieved 2018-10-10, from http://doi.wiley.com/10.1029/2010JA015347 doi: 10.1029/2010JA015347
Delamere, P. A., Wilson, R. J., Eriksson, S., & Bagenal, F. (2013, January). Magnetic signatures of Kelvin-Helmholtz vortices on Saturn's magnetopause: Global survey. *Journal of Geophysical Research: Space Physics*, *118*(1), 393–404. Retrieved 2018-10-16, from http://doi.wiley.com/10.1029/2012JA018197 doi: 10.1029/2012JA018197
Esposito, L. W., Barth, C. A., Colwell, J. E., Lawrence, G. M., McClintock, W. E., Stewart, A. I. F., ... Yung, Y. L. (2004, November). The Cassini Ultraviolet Imaging Spectrograph investigation. *Space Science Reviews*, *115*(1-4), 299–361. Retrieved 2018-06-16, from https://link.springer.com/article/10.1007/s11214-004-1455-8 doi: 10.1007/s11214-004-1455-8
Grodent, D. (2015, April). A Brief Review of Ultraviolet Auroral Emissions on Giant Planets. *Space Science Reviews*, *187*(1-4), 23–50. Retrieved 2018-04-20, from http://link.springer.com/10.1007/s11214-014-0052-8 doi: 10.1007/s11214-014-0052-8
Grodent, D., Gustin, J., Gérard, J.-C., Radioti, A., Bonfond, B., & Pryor, W. R. (2011, September). Small-scale structures in Saturn's ultraviolet aurora. *Journal of Geophysical Research: Space Physics*, *116*(A09225). Retrieved 2018-04-20, from http://doi.wiley.com/10.1029/2011JA016818 doi: 10.1029/2011JA016818
Grodent, D., Gérard, J.-C., Cowley, S. W. H., Bunce, E. J., & Clarke, J. T. (2005). Variable morphology of Saturn's southern ultraviolet aurora. *Journal of Geophysical Research*, *110*(A07215). Retrieved 2018-04-27, from http://doi.wiley.com/10.1029/2004JA010983 doi: 10.1029/2004JA010983
Grodent, D., Radioti, A., Bonfond, B., & Gérard, J.-C. (2010, August). On the origin of Saturn's outer auroral emission. *Journal of Geophysical Research: Space Physics*, *115*(A08219). Retrieved 2018-04-20, from http://doi.wiley.com/10.1029/2009JA014901 doi: 10.1029/2009JA014901
Gustin, J., Grodent, D., Radioti, A., Pryor, W., Lamy, L., & Ajello, J. (2017, March). Statistical study of Saturn's auroral electron properties with Cassini/UVIS FUV spectral images. *Icarus*, *284*, 264–283. Retrieved 2018-04-20, from http://linkinghub.elsevier.com/retrieve/pii/S0019103516304705 doi: 10.1016/j.icarus.2016.11.017
Gustin, J., Grodent, D., Ray, L., Bonfond, B., Bunce, E., Nichols, J., & Ozak, N. (2016, April). Characteristics of north jovian aurora from STIS FUV spectral images. *Icarus*, *268*, 215–241. Retrieved 2018-04-20, from http://linkinghub.elsevier.com/retrieve/pii/S0019103515006144 doi: 10.1016/j.icarus.2015.12.048
Gérard, J.-C., Bonfond, B., Gustin, J., Grodent, D., Clarke, J. T., Bisikalo, D., & Shematovich, V. (2009, January). Altitude of Saturn's aurora and its implications for the characteristic energy of precipitated electrons. *Geophysical Research Letters*, *36*(L02202). Retrieved 2018-04-24, from http://doi.wiley.com/10.1029/2008GL036554 doi: 10.1029/2008GL036554
Gérard, J.-C., Bunce, E. J., Grodent, D., Cowley, S. W. H., Clarke, J. T., & Badman, S. V. (2005). Signature of Saturn's auroral cusp: Simultaneous Hubble Space Telescope FUV observations and upstream solar wind monitoring. *Journal of Geophysical Research*, *110*(A11201). Retrieved

2018-04-20, from http://doi.wiley.com/10.1029/2005JA011094 doi: 10.1029/2005JA011094

Gérard, J.-C., Grodent, D. C., Gustin, J., Saglam, A., Clarke, J. T., & Trauger, J. T. (2004). Characteristics of Saturn's FUV aurora observed with the Space Telescope Imaging Spectrograph. *Journal of Geophysical Research*, *109*(A09207). Retrieved 2018-05-04, from http://doi.wiley.com/10.1029/2004JA010513 doi: 10.1029/2004JA010513

Hunt, G. J., Cowley, S. W. H., Provan, G., Bunce, E. J., Alexeev, I. I., Belenkaya, E. S., ... Coates, A. J. (2014, December). Field-aligned currents in Saturn's southern nightside magnetosphere: Subcorotation and planetary period oscillation components. *Journal of Geophysical Research: Space Physics*, *119*(12), 9847–9899. Retrieved 2018-04-20, from http://doi.wiley.com/10.1002/2014JA020506 doi: 10.1002/2014JA020506

Kellett, S., Arridge, C. S., Bunce, E. J., Coates, A. J., Cowley, S. W. H., Dougherty, M. K., ... Wilson, R. J. (2010, August). Nature of the ring current in Saturn's dayside magnetosphere. *Journal of Geophysical Research: Space Physics*, *115*(A08201). Retrieved 2019-03-01, from http://doi.wiley.com/10.1029/2009JA015146 doi: 10.1029/2009JA015146

Kellett, S., Arridge, C. S., Bunce, E. J., Coates, A. J., Cowley, S. W. H., Dougherty, M. K., ... Wilson, R. J. (2011, May). Saturn's ring current: Local time dependence and temporal variability. *Journal of Geophysical Research: Space Physics*, *116*(A05220). Retrieved 2018-12-10, from http://doi.wiley.com/10.1029/2010JA016216 doi: 10.1029/2010JA016216

Lamy, L., Prangé, R., Tao, C., Kim, T., Badman, S. V., Zarka, P., ... Radioti, A. (2018, September). Saturn's Northern Aurorae at Solstice From HST Observations Coordinated With Cassini's Grand Finale. *Geophysical Research Letters*, *45*(18), 9353–9362. Retrieved 2019-05-16, from http://doi.wiley.com/10.1029/2018GL078211 doi: 10.1029/2018GL078211

McAndrews, H., Thomsen, M., Arridge, C., Jackman, C., Wilson, R., Henderson, M., ... Dougherty, M. (2009, December). Plasma in Saturn's nightside magnetosphere and the implications for global circulation. *Planetary and Space Science*, *57*(14-15), 1714–1722. Retrieved 2019-10-11, from https://linkinghub.elsevier.com/retrieve/pii/S0032063309000750 doi: 10.1016/j.pss.2009.03.003

Melin, H., Stallard, T., Miller, S., Gustin, J., Galand, M., Badman, S. V., ... Baines, K. H. (2011, August). Simultaneous Cassini VIMS and UVIS observations of Saturn's southern aurora: Comparing emissions from H, H_2 and H_3^+ at a high spatial resolution. *Geophysical Research Letters*, *38*(L15203). Retrieved 2018-05-28, from http://doi.wiley.com/10.1029/2011GL048457 doi: 10.1029/2011GL048457

Mitchell, D. G., Krimigis, S. M., Paranicas, C., Brandt, P. C., Carbary, J. F., Roelof, E. C., ... Pryor, W. R. (2009, December). Recurrent energization of plasma in the midnight-to-dawn quadrant of Saturn's magnetosphere, and its relationship to auroral UV and radio emissions. *Planetary and Space Science*, *57*(14-15), 1732–1742. Retrieved 2018-04-20, from http://linkinghub.elsevier.com/retrieve/pii/S0032063309001044 doi: 10.1016/j.pss.2009.04.002

Nichols, J. D., Badman, S. V., Bunce, E. J., Clarke, J. T., Cowley, S. W. H., Hunt, G. J., & Provan, G. (2016, January). Saturn's northern auroras as observed using the Hubble Space Telescope. *Icarus*, *263*, 17–31. Retrieved 2018-04-20, from http://linkinghub.elsevier.com/retrieve/pii/S001910351500411X doi: 10.1016/j.icarus.2015.09.008

Nichols, J. D., Clarke, J. T., Cowley, S. W. H., Duval, J., Farmer, A. J., Gérard, J.-C., ... Wannawichian, S. (2008, November). Oscillation of Saturn's southern auroral oval. *Journal of Geophysical Research: Space Physics*, *113*(A11205).

Retrieved 2018-04-20, from http://doi.wiley.com/10.1029/2008JA013444 doi: 10.1029/2008JA013444

Paranicas, C., Thomsen, M., Achilleos, N., Andriopoulou, M., Badman, S., Hospodarsky, G., … Sergis, N. (2016, January). Effects of radial motion on interchange injections at Saturn. *Icarus*, *264*, 342–351. Retrieved 2019-09-23, from https://linkinghub.elsevier.com/retrieve/pii/S0019103515004686 doi: 10.1016/j.icarus.2015.10.002

Pryor, W. R., Esposito, L. W., Jouchoux, A., West, R. A., Grodent, D., Gérard, J., … Koskinen, T. (2019, July). Cassini UVIS Detection of Saturn's North Polar Hexagon in the Grand Finale Orbits. *Journal of Geophysical Research: Planets*, *124*, 1979–1988. Retrieved 2019-08-22, from https://onlinelibrary.wiley.com/doi/abs/10.1029/2019JE005922 doi: 10.1029/2019JE005922

Radioti, A., Grodent, D., Gérard, J.-C., & Bonfond, B. (2010, July). Auroral signatures of flow bursts released during magnetotail reconnection at Jupiter. *Journal of Geophysical Research: Space Physics*, *115*(A07214). Retrieved 2019-09-05, from http://doi.wiley.com/10.1029/2009JA014844 doi: 10.1029/2009JA014844

Radioti, A., Grodent, D., Gérard, J.-C., Bonfond, B., & Clarke, J. T. (2008, February). Auroral polar dawn spots: Signatures of internally driven reconnection processes at Jupiter's magnetotail. *Geophysical Research Letters*, *35*(L03104). Retrieved 2019-09-05, from http://doi.wiley.com/10.1029/2007GL032460 doi: 10.1029/2007GL032460

Radioti, A., Grodent, D., Gérard, J.-C., Bonfond, B., Gustin, J., Pryor, W., … Arridge, C. S. (2013, September). Auroral signatures of multiple magnetopause reconnection at Saturn. *Geophysical Research Letters*, *40*(17), 4498–4502. Retrieved 2018-04-20, from http://doi.wiley.com/10.1002/grl.50889 doi: 10.1002/grl.50889

Radioti, A., Grodent, D., Gérard, J.-C., Milan, S. E., Bonfond, B., Gustin, J., & Pryor, W. (2011, November). Bifurcations of the main auroral ring at Saturn: ionospheric signatures of consecutive reconnection events at the magnetopause. *Journal of Geophysical Research: Space Physics*, *116*(A11209). Retrieved 2018-04-20, from http://doi.wiley.com/10.1029/2011JA016661 doi: 10.1029/2011JA016661

Radioti, A., Grodent, D., Jia, X., Gérard, J.-C., Bonfond, B., Pryor, W., … Jackman, C. (2016, January). A multi-scale magnetotail reconnection event at Saturn and associated flows: Cassini/UVIS observations. *Icarus*, *263*, 75–82. Retrieved 2018-04-20, from http://linkinghub.elsevier.com/retrieve/pii/S0019103514006964 doi: 10.1016/j.icarus.2014.12.016

Radioti, A., Grodent, D., Yao, Z. H., Gérard, J.-C., Badman, S. V., Pryor, W., & Bonfond, B. (2017, December). Dawn Auroral Breakup at Saturn Initiated by Auroral Arcs: UVIS/Cassini Beginning of Grand Finale Phase. *Journal of Geophysical Research: Space Physics*, *122*(12), 12,111–12,119. Retrieved 2018-04-20, from http://doi.wiley.com/10.1002/2017JA024653 doi: 10.1002/2017JA024653

Radioti, A., Tomás, A. T., Grodent, D., Gérard, J.-C., Gustin, J., Bonford, B., … Menietti, J. D. (2009, April). Equatorward diffuse auroral emissions at Jupiter: Simultaneous HST and Galileo observations. *Geophysical Research Letters*, *36*(L07101). Retrieved 2018-04-20, from http://doi.wiley.com/10.1029/2009GL037857 doi: 10.1029/2009GL037857

Radioti, A., Yao, Z., Grodent, D., Palmaerts, B., Roussos, E., Dialynas, K., … Bonfond, B. (2019, October). Auroral Beads at Saturn and the Driving Mechanism: *Cassini* Proximal Orbits. *The Astrophysical Journal*, *885*(1), L16. Retrieved 2019-11-09, from https://iopscience.iop.org/article/10.3847/2041-8213/ab4e20 doi: 10.3847/2041-8213/ab4e20

Schippers, P., Blanc, M., André, N., Dandouras, I., Lewis, G. R., Gilbert, L. K., … Dougherty, M. K. (2008, July). Multi-instrument analysis of electron populations in Saturn's magnetosphere. *Journal of Geophysical Research: Space Physics*, *113*(A07208). Retrieved 2019-08-02, from http://doi.wiley.com/10.1029/2008JA013098 doi: 10.1029/2008JA013098

Stallard, T., Miller, S., Lystrup, M., Achilleos, N., Bunce, E. J., Arridge, C. S., … Drossart, P. (2008, November). Complex structure within Saturn's infrared aurora. *Nature*, *456*, 214–217. Retrieved 2018-10-16, from http://www.nature.com/articles/nature07440 doi: 10.1038/nature07440

Stallard, T., Miller, S., Melin, H., Lystrup, M., Dougherty, M., & Achilleos, N. (2007, July). Saturn's auroral/polar H+3 infrared emission: I. General morphology and ion velocity structure. *Icarus*, *189*(1), 1–13. Retrieved 2018-04-23, from http://linkinghub.elsevier.com/retrieve/pii/S0019103507000231 doi: 10.1016/j.icarus.2006.12.027

Talboys, D. L., Arridge, C. S., Bunce, E. J., Coates, A. J., Cowley, S. W. H., Dougherty, M. K., & Khurana, K. K. (2009, October). Signatures of field-aligned currents in Saturn's nightside magnetosphere. *Geophysical Research Letters*, *36*(L19107). Retrieved 2018-10-16, from http://doi.wiley.com/10.1029/2009GL039867 doi: 10.1029/2009GL039867

Thomsen, M. F., Mitchell, D. G., Jia, X., Jackman, C. M., Hospodarsky, G., & Coates, A. J. (2015, April). Plasmapause formation at Saturn: Plasmapause Formation at Saturn. *Journal of Geophysical Research: Space Physics*, *120*(4), 2571–2583. Retrieved 2019-09-23, from http://doi.wiley.com/10.1002/2015JA021008 doi: 10.1002/2015JA021008

Thomsen, M. F., Reisenfeld, D. B., Delapp, D. M., Tokar, R. L., Young, D. T., Crary, F. J., … Williams, J. D. (2010, October). Survey of ion plasma parameters in Saturn's magnetosphere. *Journal of Geophysical Research: Space Physics*, *115*(A10220). Retrieved 2019-06-15, from http://doi.wiley.com/10.1029/2010JA015267 doi: 10.1029/2010JA015267

Tripathi, A. K., Singhal, R. P., & Singh, O. N. (2018, May). The Generation of Saturn's Aurora at Lower Latitudes by Electrostatic Waves. *Journal of Geophysical Research: Space Physics*, *123*(5), 3565–3579. Retrieved 2019-09-06, from http://doi.wiley.com/10.1002/2017JA024804 doi: 10.1002/2017JA024804

Vampola, A. L., & Gorney, D. J. (1983). Electron energy deposition in the middle atmosphere. *Journal of Geophysical Research*, *88*(A8), 6267. Retrieved 2019-09-06, from http://doi.wiley.com/10.1029/JA088iA08p06267 doi: 10.1029/JA088iA08p06267

Wilson, R. J., Bagenal, F., & Persoon, A. M. (2017, July). Survey of thermal plasma ions in Saturn's magnetosphere utilizing a forward model. *Journal of Geophysical Research: Space Physics*, *122*(7), 7256–7278. Retrieved 2019-07-24, from http://doi.wiley.com/10.1002/2017JA024117 doi: 10.1002/2017JA024117

Figure 1.

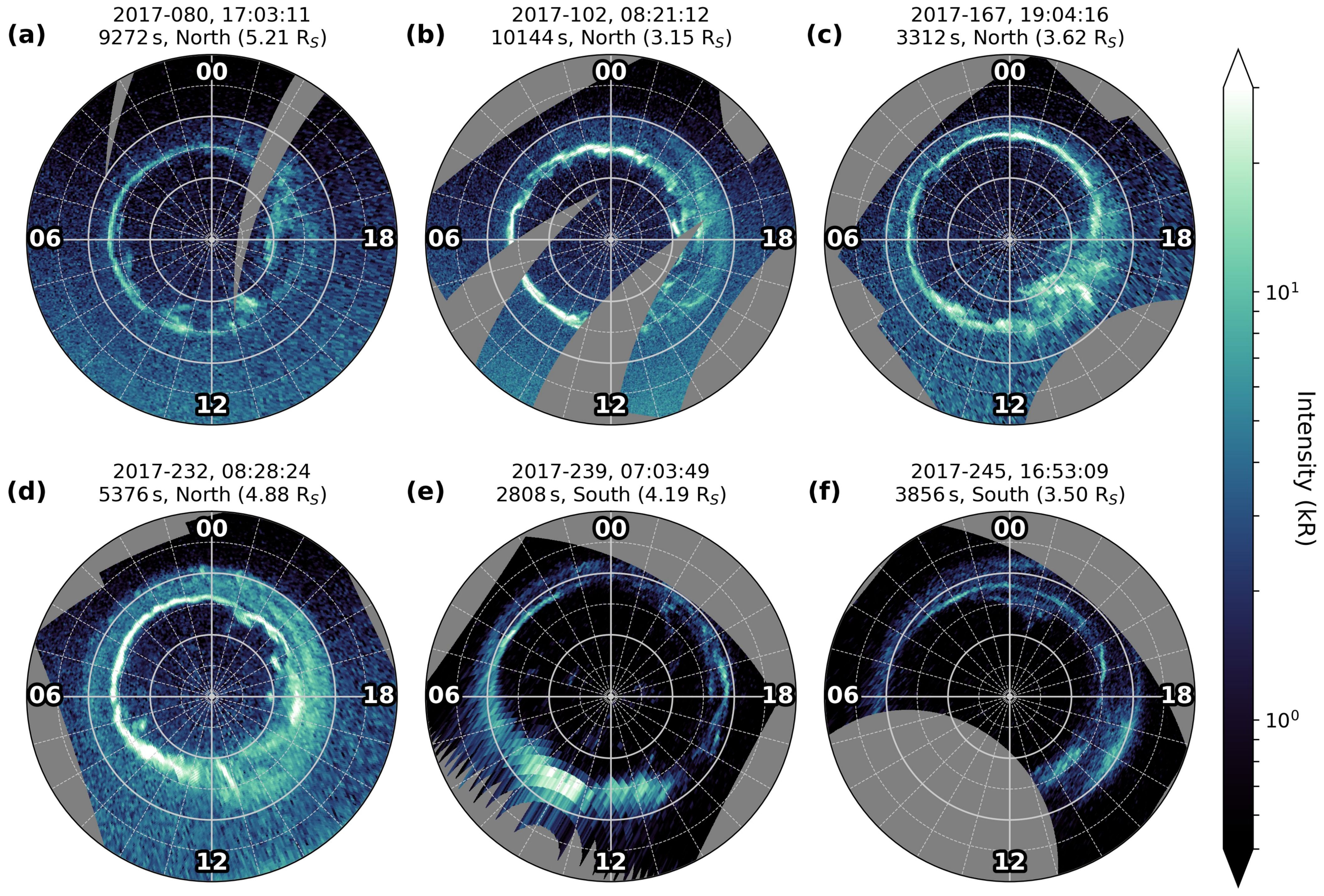
(a)
2017-080, 17:03:11
9272 s, North (5.21 R$_S$)
(b)
2017-102, 08:21:12
10144 s, North (3.15 R$_S$)
(c)
2017-167, 19:04:16
3312 s, North (3.62 R$_S$)
(d)
2017-232, 08:28:24
5376 s, North (4.88 R$_S$)
(e)
2017-239, 07:03:49
2808 s, South (4.19 R$_S$)
(f)
2017-245, 16:53:09
3856 s, South (3.50 R$_S$)
00
06
12
18
Intensity (kR)
10^1
10^0

Figure 2.

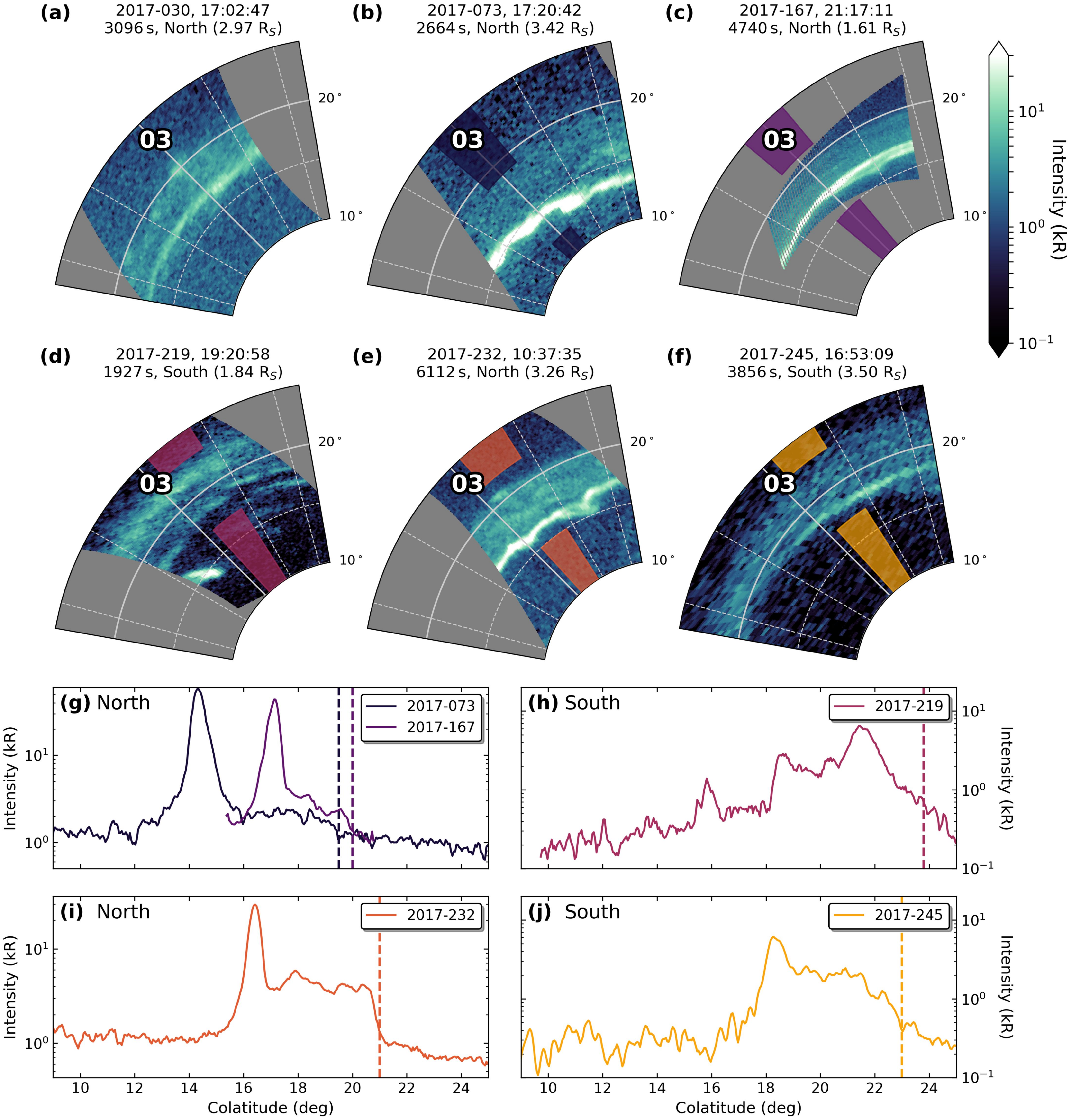

(a) 2017-030, 17:02:47
3096 s, North (2.97 R$_S$)
(b) 2017-073, 17:20:42
2664 s, North (3.42 R$_S$)
(c) 2017-167, 21:17:11
4740 s, North (1.61 R$_S$)
(d) 2017-219, 19:20:58
1927 s, South (1.84 R$_S$)
(e) 2017-232, 10:37:35
6112 s, North (3.26 R$_S$)
(f) 2017-245, 16:53:09
3856 s, South (3.50 R$_S$)
03
20°
10°
Intensity (kR)
(g) North
2017-073
2017-167
(h) South
2017-219
(i) North
2017-232
(j) South
2017-245
Colatitude (deg)

Figure 3.

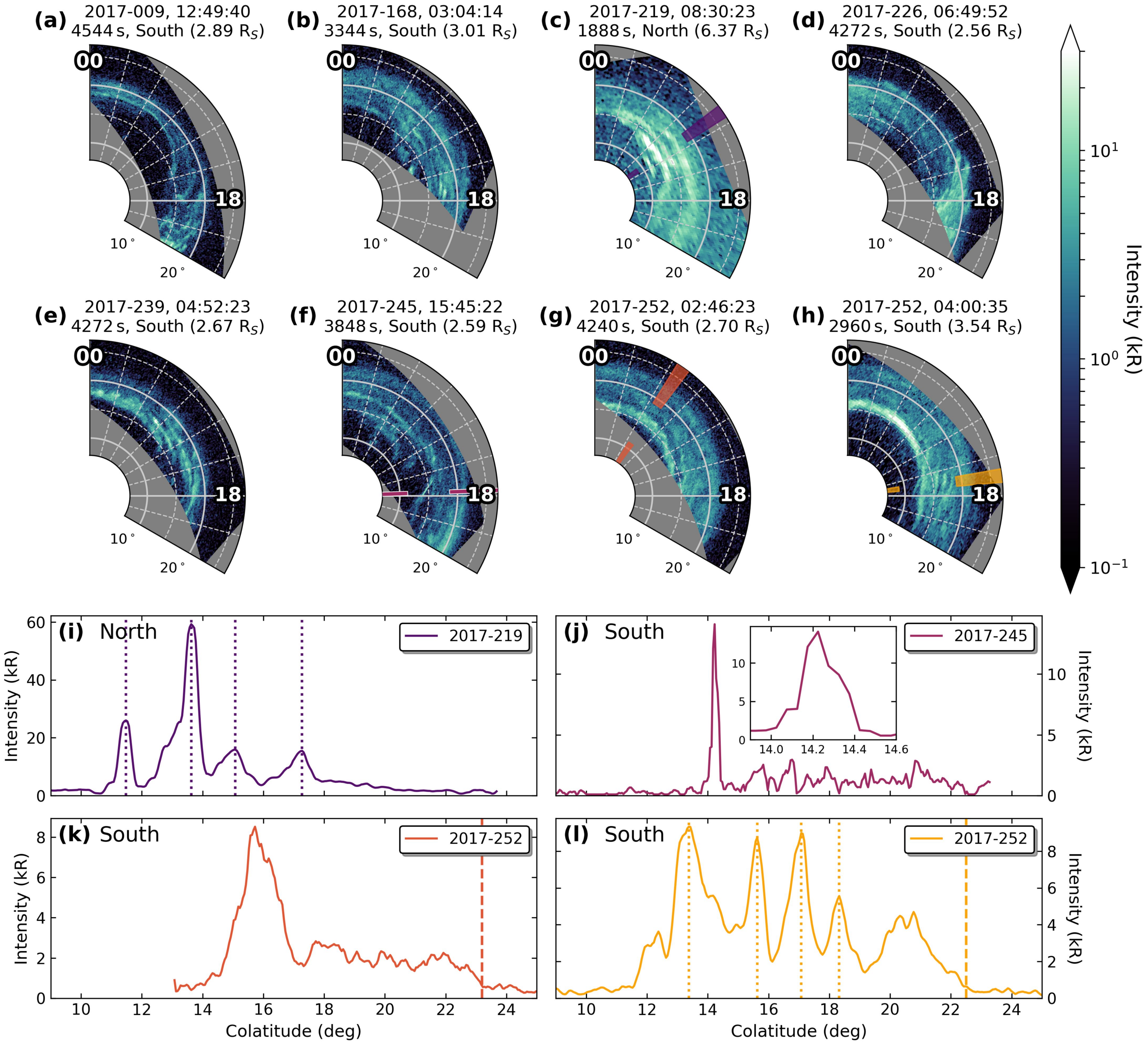

(a) 2017-009, 12:49:40
4544 s, South (2.89 R_S)
(b) 2017-168, 03:04:14
3344 s, South (3.01 R_S)
(c) 2017-219, 08:30:23
1888 s, North (6.37 R_S)
(d) 2017-226, 06:49:52
4272 s, South (2.56 R_S)
(e) 2017-239, 04:52:23
4272 s, South (2.67 R_S)
(f) 2017-245, 15:45:22
3848 s, South (2.59 R_S)
(g) 2017-252, 02:46:23
4240 s, South (2.70 R_S)
(h) 2017-252, 04:00:35
2960 s, South (3.54 R_S)
00
18
10°
20°
Intensity (kR)
(i) North
2017-219
(j) South
2017-245
(k) South
2017-252
(l) South
2017-252
Intensity (kR)
Colatitude (deg)

Figure 4.

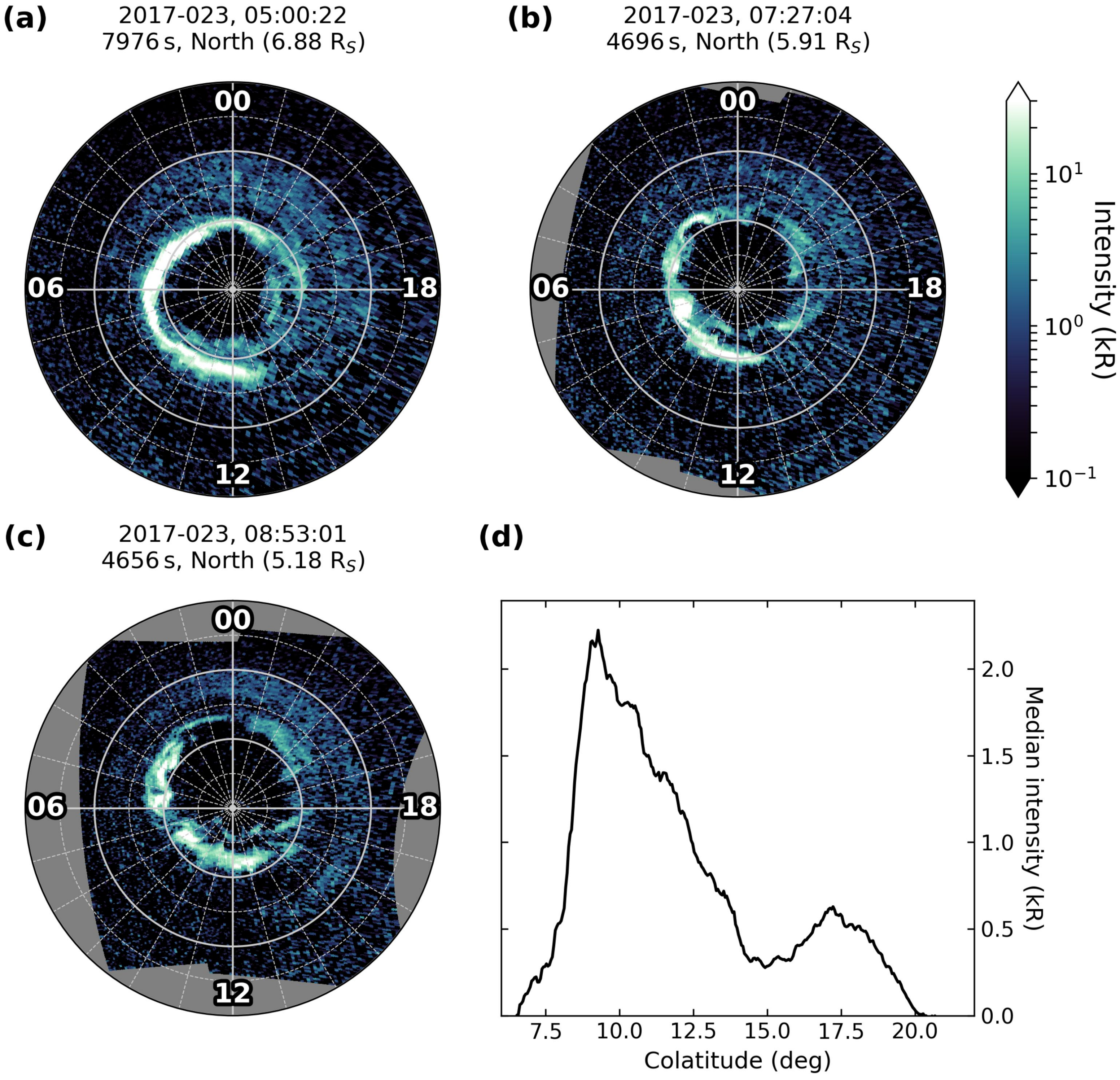

(a)
2017-023, 05:00:22
7976 s, North (6.88 R$_S$)
(b)
2017-023, 07:27:04
4696 s, North (5.91 R$_S$)
(c)
2017-023, 08:53:01
4656 s, North (5.18 R$_S$)
(d)
00
06
18
12
Intensity (kR)
10^{1}
10^{0}
10^{-1}
Median intensity (kR)
0.0
0.5
1.0
1.5
2.0
7.5
10.0
12.5
15.0
17.5
20.0
Colatitude (deg)